Structure-Performance Relationship in Ziegler-Natta Olefin Polymerization with Novel Core-Shell $MgO/MgCl_2/TiCl_4$ Catalysts

Toshiaki Taniike, Patchanee Chammingkwan, and Minoru Terano*

School of Materials Science, Japan Advance Institute of Science and Technology, 1-1 Asahidai, Nomi, Ishikawa 923-1292, Japan

*CORRESPONDING AUTHOR

Tel: +81-761-51-1620; Fax: +81-761-51-1625; E-mail: terano@jaist.ac.jp

ABSTRACT: The impact of support architectures on the olefin polymerization performance of heterogeneous Ziegler-Natta catalysts has been scarcely understood due to the complexity of pore system and the fragmentation-induced structural changes during polymerization. In this communication, a series of novel core-shell $MgO/MgCl_2/TiCl_4$ catalysts were synthesized by utilizing poreless single-crystal MgO nanoparticles as a non-fragmentable core material. Employing these catalysts, we have successfully established a structure-performance relationship (SPR) that the propylene polymerization activity is perfectly proportional to the catalyst surface area for the first time. On the other hand, polymer properties were found to be decided by active site natures independently of the surface area.

KEYWORDS: Ziegler-Natta polymerization; polyolefins; structure-performance relationship; core-shell; nanoparticle

1. Introduction

Elucidation of the structure-performance relationship (SPR) is one of the ultimate goals for systematic and tailored design of advanced materials. In heterogeneous catalysis, both active site structures and support architectures either competitively or synergistically contribute to catalytic performances. For example, a linear relationship between catalyst surface area and activity has been found in many catalytic systems, like in photocatalytic decomposition of aldehyde on Bi_2WO_6 [1]. The pore dimension of support materials can affect both activity and selectivity through restricted diffusion and formation of bulkier molecules, *e.g.* the pore size of mesoporous silicate regulates the alkylation degree of benzene [2]. As was demonstrated in CO oxidation on Pt surfaces [3], catalytic performance are often very sensitive to surface structures (plane and defect), which is especially important in shaping metal nanoparticles, and vice versa.

In heterogeneous Ziegler-Natta (ZN) catalysts ($TiCl_4$ supported on $MgCl_2$) for olefin polymerization, SPR for active sites has been gradually uncovered as a result of tremendous efforts. For instance, ethylene can be polymerized irrespective of the oxidation state of Ti species, while Ti^{2+} species is inactive for polymerization of α-olefin [4]. The polymer molecular weight tends to be larger for a lower oxidation state [4]. Stereoselectivity in propylene polymerization is influenced by the presence or absence of bulky ligands at metal sites adjacent to a Ti center, as was proposed in the three-site model [5,6]. On the contrary, SPR for support architectures has been scarcely established in the long history, even for the most basic SPR between the catalyst surface area and activity. Gerbasi et al. [7] plotted the ethylene polymerization activity of a $TiCl_4/MgCl_2$ catalyst along the grinding time, where the activity was correlated with the structural disorder of $MgCl_2$ support rather than the catalyst surface area.

Marigo et al. [8] evaluated the surface areas of several ZN catalysts prepared from $MgCl_2$-alcohol adduct by means of the BET analysis in N_2 adsorption and small-angle X-ray scattering (SAXS). They found that the propylene polymerization activity was never correlated with the BET surface area, while some level of correlation was found for the SAXS surface area. However, the obtained correlation was rather rough and could not be extrapolated to the origin (*i.e.* zero activity at zero surface area) plausibly due to the contribution of closed pores to the SAXS surface area. This result implies an intrinsic problem to apply the BET analysis to the surface area of typical ZN catalysts. Bozik et al. [9] examined the ethylene polymerization activities of various metallophosphate-supported $TiCl_4$ catalysts. They suggested the presence of some but very rough correlation (R^2~0.8) between the activity and the BET surface area. Beside the surface area, the importance of pore architectures of $MgCl_2$ support has been empirically recognized. Nevertheless, their influences on polymerization have been hardly studied in a quantitative manner owing to the shape irregularity and size distribution of pore structures. Furthermore, the fragmentation of catalyst particles (which consist of hierarchically agglomerated smaller structural units) causes time-course variations of support architectures during polymerization, thus messing up the initially characterized architectures. Since the performance of a ZN catalyst results from interplay among the polymerization reaction on catalyst surfaces, the monomer transportation within pores and the particle fragmentation during polymerization, it is almost impossible to explore clear SPR using a typical industrial ZN catalyst.

In this communication, we report the first SPR establishment for support architectures of heterogeneous ZN catalysts on the basis of novel core-shell $MgO/MgCl_2/TiCl_4$ catalysts.

Starting from single-crystal MgO nanoparticles with various dimensions and surface areas, a series of core-shell $MgO/MgCl_2/TiCl_4$ catalysts were fabricated, where poreless and non-fragmentable MgO core was thinly covered by the catalytic components. While these catalysts exhibited active site natures typical for $MgCl_2$-supported ZN catalysts in propylene polymerization, the poreless and non-fragmentable features gave a perfectly proportional relation between the catalyst surface area and activity.

2. Experimental

2.1. Materials

Analytical grades of magnesium nitrate hexahydrate ($Mg(NO)_2 \cdot 6H_2O$) and oxalic acid dihydrate ($(COOH)_2 \cdot 2H_2O$) purchased from Wako Pure Chemical Industries, Ltd. were used as the precursors for the synthesis of MgO. Anhydrous ethanol and titanium tetrachloride ($TiCl_4$) purchased from Wako Pure Chemical Industries, Ltd. and triisobutyl aluminum (TiBA) donated by Tosoh FineChem Co., Ltd. were used as received. Heptane was used after dehydration by passing through a column of molecular sieve 4A. Propylene of research grade was used without further purification.

2.2. Preparation of MgO nanoparticles

Single-crystal MgO nanoparticles were synthesized according to the sol-gel method described by Kumar and Kumar [10]. $Mg(NO)_2 \cdot 6H_2O$ and $(COOH)_2 \cdot 2H_2O$ were dissolved separately in ethanol. The two precursors were mixed at the molar ratio of 1:1 to form white gel. The gel was digested for 12 h under vigorous mixing and dried at 100ºC for 24 h to form $MgC_2O_4 \cdot 2H_2O$.

The dried gel was then calcined in air at 800, 750, 700, 650 and 500ºC to obtain MgO nanoparticles having different sizes and surface areas, denoted as MgO1, MgO2, MgO3, MgO4 and MgO5, respectively.

2.3. Preparation of $MgO/MgCl_2/TiCl_4$ catalyst

2.0 g of MgO powder was thermally pre-treated at 130°C under nitrogen flow for 6 h to remove physisorbed water, and subsequently treated with 30 ml of refluxing $TiCl_4$ at 140°C for 2 h. The solid was washed with heptane 10 times and kept as slurry under nitrogen.

2.4. Polymerization

Propylene polymerization was performed in a 1 L stainless steel autoclave equipped with a mechanical stirrer. 200 ml of heptane as solvent was introduced to the reactor under nitrogen and then saturated with 0.5 MPa of propylene at 50ºC for 30 min. Following the addition of 2.0 mmol of TiBA as an activator, 30 mg of a catalyst was charged to the reactor to start polymerization. The polymerization was continued for 30 min at the constant pressure and temperature, and finally terminated by the addition of acidic ethanol.

2.5. Characterizations

Powder X-ray diffraction (XRD, RINT 2100, Rigaku) was used to identify and determine the crystallite structures and dimensions of MgO and $MgO/MgCl_2/TiCl_4$ particles. Transmission electron microscope (TEM) was recorded on Hitachi H-7100 for the observation of particle morphology. N_2 adsorption/desorption experiments were conducted on Belsorp-max at 77 K to

determine the surface area based on the BET method.

The molecular weight (M_n) of produced polypropylene (PP) was measured by gel permeation chromatography (GPC, Viscotek, HT-GPC 350) with Shodex UT-806M columns at 140ºC using *o*-dichlorobenzene as solvent. The stereostructure of PP was analyzed by ^{13}C NMR (Bruker 400 MHz NMR spectrometer) at 120ºC using 1,1,2,2-tetrachloroethane-d_2 as an internal lock and reference.

3. Results and discussion

Fig. 1 shows representative TEM images of MgO1-5 synthesized by the sol-gel method and subsequent calcination at different temperatures. The particles were dense with cubic and partially polygonal shapes for all the samples. They were separated from each other with relatively uniform sizes ranging approximately 8-35 nm according to the calcination temperature. At a higher calcination temperature, particles were larger due to thermally-driven particle growth. The formation of MgO pure phase with a cubic crystal structure was confirmed by XRD for all the samples (not shown). Table 1 lists the crystallite sizes estimated from the (200) diffraction peak of MgO using the Scherrer equation along with the BET surface areas. The crystallite sizes increased from 8 to 32 nm as the calcination temperature increased. The quantitative coincidence between the crystallite sizes and the particle sizes in TEM indicated that the MgO nanoparticles were single-crystal. The change in the specific surface area was also correlated with the crystallite sizes, where a larger crystallite size led to a lower surface area. The particle sizes estimated from the BET surface areas under the assumption of a cubic shape (Table 1) again well coincided with the sizes obtained from XRD and TEM except for MgO1.

This fact suggested that the single-crystal MgO nanoparticles were uniform in size and free from internal pore structures. The substantially greater size estimated from the BET surface area for MgO1 was due to the deviation from the cubic shape. The reiterated calculation with the assumption of a spherical shape resulted in a smaller size than the XRD and TEM sizes, indicating that MgO1 could have an intermediate shape between cubic and spherical, consistently with the polygonal shape observed in TEM. In this way, a series of poreless single-crystal MgO nanoparticles were obtained with the surface area systematically altered by the calcination temperature.

The MgO nanoparticles with well-defined architectures were chlorinated and titanated with refluxing $TiCl_4$ to synthesize core-shell $MgO/MgCl_2/TiCl_4$ catalysts. The Ti content increased with the increase of the MgO surface area (Table 1). The XRD patterns of the obtained catalysts are shown in Fig. 2. Beside five prominent peaks of MgO pure phase at 37º, 43º, 62º, 74º and 78º (which correspond to (111), (200), (220), (331) and (222) reflections [10]), MgO1-4/$MgCl_2$/$TiCl_4$ catalysts exhibited minor and broad peaks, characteristic of anhydrous δ-$MgCl_2$, at around 15º, 30-35º and 50º [11]. The crystallite sizes of MgO cores calculated from the XRD patterns as well as the BET surface areas were almost kept unchanged before and after the $TiCl_4$ treatment. These facts suggested that thin $MgCl_2$ overlayer was formed on the MgO core without altering the particle structures of MgO. The uniform sizes of MgO nanoparticles observed in the TEM images let us to presume that the formation of the $MgCl_2$ overlayer and immobilization of Ti species on the surfaces occurred homogenously, following the reaction schemes proposed by Tatizawa et al. [12],

$$MgO + TiCl_4 \rightarrow MgCl_2 + TiOCl_2 \quad (1),$$

$MgO + 2TiCl_4 \rightarrow MgCl_2 \cdot TiCl_4 + TiOCl_2$ (2).

On the contrary to MgO1-4/$MgCl_2$/$TiCl_4$, MgO5/$MgCl_2$/$TiCl_4$ exhibited sharp diffraction peaks at $2\theta \approx 15^\circ$, 30°, 35° and 50°, corresponding to the Miller indices of (003), (012), (104) and (110) of α-$MgCl_2$, respectively [8], while the characteristic peaks of MgO almost disappeared. Correspondingly, the surface area of MgO5/$MgCl_2$/$TiCl_4$ significantly decreased from 221.5 to 47.0 m^2/g. Hence, the smallest MgO5 particles underwent deep chlorination into the bulk and were mostly converted into α-$MgCl_2$, which accompanied sintering and agglomeration of the particles. Due to the loss of the original particle structures, MgO5/$MgCl_2$/$TiCl_4$ was excluded in the following polymerization experiments.

Fig. 3 shows the propylene polymerization activity of the core-shell MgO/$MgCl_2$/$TiCl_4$ catalysts (except sintered MgO5). The activity (per g of catalyst) was found to be completely proportional to the catalyst surface area, crossing the origin (Fig. 3). At our best knowledge, this is the first experimental results on a linear relationship between the surface area and activity, while typical ZN catalysts suffer from the fragmentation phenomena, the complexity of pore architectures, and so on. On the contrary, the Ti content (which did not linearly increase with the catalyst surface area (Table 1)) was not clearly correlated with the activity, even though a higher Ti content was expected to give a higher activity. It was presumed that active site concentration per surface area reaches a plateau in the presence of excess alkylaluminum, resulting in a constant yield per surface area. The polymer properties were quite insensitive to the support variables (Table 2), suggesting that active sites are situated in similar environments on the surfaces of the catalysts: the stereoregularities were similarly about 50 mol% in *mmmm* and M_n was in a range of 2.7-3.1 $\times 10^4$ g/mol with the M_w/M_n values of 6.1-6.8, both of which were

typical values for donor-free $TiCl_4/MgCl_2$ catalysts. It was concluded that the core-shell $MgO/MgCl_2/TiCl_4$ catalysts reproduce the active site environments of typical ZN catalysts, but the novelty of their poreless and non-fragmentable structures has enabled the establishment of the first clear SPR for support architectures in heterogeneous ZN olefin polymerization.

4. Conclusions

A series of poreless single-crystal MgO nanoparticles with different sizes were prepared by the sol-gel method. The MgO nanoparticles were utilized as a non-fragmentable core material to prepare novel core-shell $MgO/MgCl_2/TiCl_4$ catalysts for olefin polymerization. Characterization of the MgO nanoparticles and $MgO/MgCl_2/TiCl_4$ catalysts demonstrated the formation of $TiCl_4/\delta$-$MgCl_2$ overlayer without the shrinkage of MgO core except MgO5, which underwent deep chlorination into bulk and severely agglomerated. With these core-shell $MgO/MgCl_2/TiCl_4$ catalysts, SPR between the catalyst surface area and propylene polymerization activity was successfully acquired. We concluded that the catalyst surface area is primarily important for olefin polymerization activity, while polymer properties are dependent mainly on active site structures.

Acknowledgement

The Authors appreciate Japan Polychem Co., Mitsui Chemicals, Inc., Sumitomo Chemical Co., Ltd., Toho Titanium Co., Ltd., and Tosoh Finechem Co. for the donation of reagents.

References

[1] F. Amano, K. Nogami, B. Ohtani, Langmuir 26 (2010) 7174.

[2] X. Hu, M.L. Foo, G.Kh. Chuah, S. Jeanicke, J. Catal. 412 (2000) 195.

[3] K. Nakao, S. Ito, K. Tomishige, K. Kunimori, J. Phys. Chem. B 109 (2005) 17579.

[4] D. Fregonese, S. Mortara, S. Bresadola, J. Mol. Catal. A: Chem. 172 (2001) 89.

[5] V. Busico, R. Cipullo, G. Monaco, G. Talarico, M. Vacatello, J.C. Chadwick, A.L. Segre, O. Sudmeijer, Macromolecules 32 (1999) 4173.

[6] B. Liu, T. Nitta, H. Nakatani, M. Terano, Macromol. Chem. Phys. 204 (2003) 395.

[7] R. Gerbasi, A. Marigo, A. Martorana, R. Zannetti, G.P. Guidetti, G. Baruzzi, Eur. Polym. J. 20 (1984) 967.

[8] A. Marigo, C. Marega, R. Zannetti, G. Morini, G. Ferrara, Eur. Polym. J. 36 (2000) 1921.

[9] J.E. Bozik, R.F. Vogel, Y.V. Kissin, D.L. Beach, J. Appl. Polym. Sci. 29 (1984) 3491.

[10] A. Kumar, J. Kumar, J. Phys. Chem. Solids 69 (2008) 2764.

[11] J.C.J. Bart, J. Mater. Sci. 28 (1993) 278.

[12] N. Tatizawa, R. Quijada, Eur. Polym. J. 28 (1992) 139.

Figure captions

Fig. 1. TEM images of MgO particles: (a) MgO1, (b) MgO2, (c) MgO3, (d) MgO4 and (e) MgO5

Fig. 2. XRD patterns of $MgO/MgCl_2/TiCl_4$ catalysts: (a) $MgO1/MgCl_2/TiCl_4$, (b) $MgO2/MgCl_2/TiCl_4$, (c) $MgO3/MgCl_2/TiCl_4$, (d) $MgO4/MgCl_2/TiCl_4$ and (e) $MgO5/MgCl_2/TiCl_4$

Fig. 3. Relationship between the catalyst surface area and propylene polymerization activity. The color code is the same as for Fig. 2.

Table 1

Characterization results for MgO nanoparticles and $MgO/MgCl_2/TiCl_4$ catalysts.

Sample	MgO nanoparticles			$MgO/MgCl_2/TiCl_4$ catalyst	
	Crystal size in XRD[a] [nm]	BET surface area [m^2/g]	Particle size in BET[b] [nm]	BET surface area [m^2/g]	Ti content[d] [wt.-%]
MgO1	32.0 (30.3[c])	32.6	51.4 (20.7[c])	32.7	0.88
MgO2	19.5	72.9	23.0	99.8	2.39
MgO3	16.3	103.4	16.2	106.8	6.16
MgO4	12.8	128.7	13.0	148.5	7.72
MgO5	8.0	221.5	7.6	47.0	9.16

[a] Based on the Scherrer equation for the (200) peak of MgO ($K = 0.94$ for cubic crystal).

[b] Based on $d_p = 6\times10^3/S_{BET}\cdot\rho$ for cubic particles, where S_{BET} is the BET surface area and ρ is the density of MgO (3.58 g/cm^3).

[c] Assuming spherical particles.

[d] Measured by titration.

Table 2

Results of polymer analyses.

Catalyst	*mmmm*[a] [mol%]	M_n[b] [g/mol]	M_w/M_n[b]
MgO1/MgO/$TiCl_4$	52.7	3.0×10^4	6.8
MgO2/MgO/$TiCl_4$	49.4	2.7×10^4	6.8
MgO3/MgO/$TiCl_4$	50.8	3.1×10^4	6.1
MgO4/MgO/$TiCl_4$	50.0	2.7×10^4	6.7

[a] Determined with ^{13}C-NMR.

[b] Determined with GPC.

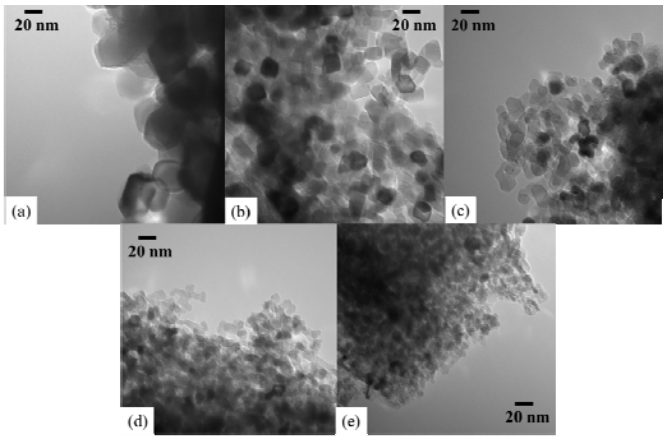
20 nm
(a)
20 nm
(b)
20 nm
(c)
20 nm
(d)
(e)
20 nm

Fig. 1.

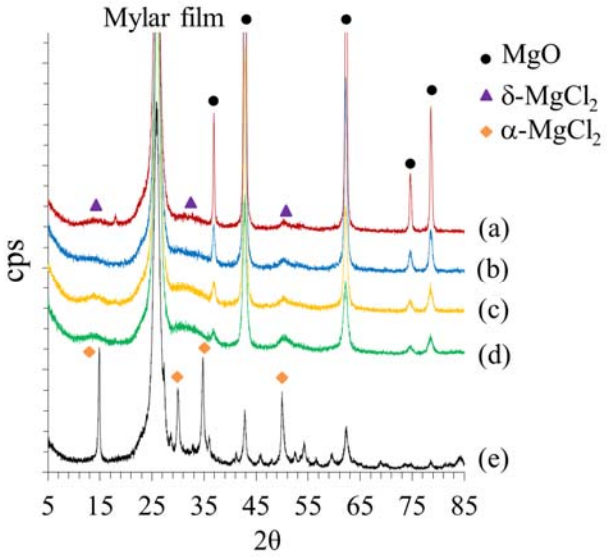
Mylar film
MgO
δ-MgCl2
α-MgCl2
(a)
(b)
(c)
(d)
(e)
cps
5
15
25
35
45
55
65
75
85
2θ

Fig. 2.

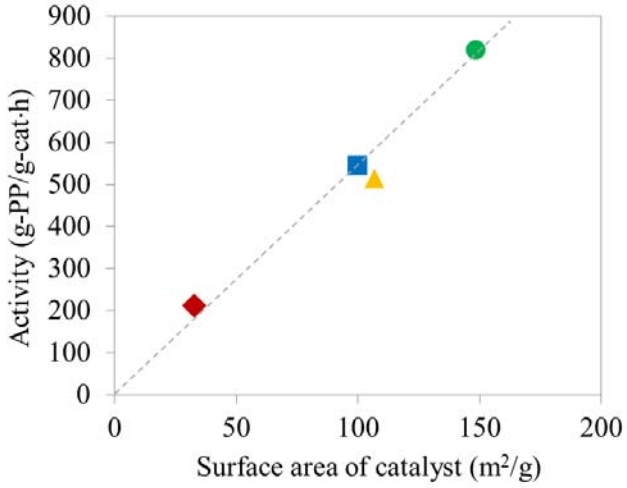
900
800
700
600
500
400
300
200
100
0
Activity (g-PP/g-cat·h)
0
50
100
150
200
Surface area of catalyst (m²/g)

Fig. 3.